Revision 1

The low-temperature shift of antigorite dehydration in the presence of sodium chloride: *in situ* diffraction study up to 3 GPa and 700 °C

Anna Yu. Likhacheva, Sergey V. Rashchenko, Anna I. Semerikova, Alexander V. Romanenko, Konstantin Glazyrin, Oleg G. Safonov

Abstract

The dehydration of serpentine mineral antigorite, $Mg_{2.8}Si_2O_5(OH)_{3.6}$, is regarded as the key step in metamorphic transformation of ultramafic hydrated rocks in subduction zones, which affects seismicity and feeds volcanic activity. The abundance of alkali-chloride brines derived from the deep subduction/upper mantle sources implies the possibility of a large control of the H_2O activity by the dissolved salts. The present study examines the effect of alkali chlorides, lowering the H_2O activity in fluid, on antigorite stability at high pressure. The decomposition of natural antigorite (Ural) in the presence of saturated NaCl-H_2O fluid was studied up to 3 GPa and 700 °C by *in-situ* X-ray diffraction combined with resistively heated diamond anvil cell. Reference experiments were also performed on salt-free sample. At 1.5-3 GPa in the presence of NaCl-saturated fluid ($X_{NaCl} \approx 0.15$) antigorite decomposes to an intermediate product assemblage of talc+forsterite at about 550 °C, which is ≈150 °C lower compared to salt-free H_2O-unsaturated system. Such low-temperature shift supports the previous models of a broadened *P-T* area of serpentinite dehydration in subducting slab. In addition, the present experiments reveal active dissolution of the product Mg silicates, first of all forsterite, in the NaCl-H_2O fluid at 600-700 °C / 1.5-3 GPa. This implies that dehydrated serpentinites are a potential source of fluids enriched in MgO and SiO_2, which play an important role in deep metasomatic processes.

Key words: antigorite; decomposition; subduction zone; NaCl aqueous fluid; H_2O activity; high pressure; high temperature; in situ X-ray diffraction.

INTRODUCTION

The serpentine group minerals, phyllosilicates with ideal formula $Mg_3Si_2O_5(OH)_4$, are major constituents of hydrated ultramafic rocks of the oceanic lithosphere. Their crystal structure, based on 1:1 tetrahedral-octahedral layers, varies from wave-shaped modulated layers in antigorite (Zussman 1954; Mellini et al. 1987), flat layers in lizardite (Mellini 1982) and rolled layers in chrysotile (Wicks and Whittaker 1975). Among these varieties, antigorite (Atg) is stable at high pressure (H*P*) and high temperature (H*T*), which makes it the main participant of the H*P*-H*T* metamorphic reactions in serpentinites. In particular, Atg dehydration is regarded as the key reaction in the transformation of serpentinites in subduction zones, since it serves as source of a large amount of water for melting in the mantle wedge and arc volcanism (Schmidt and Poli 1998). This justifies a great interest to the H*P*-H*T* stability of antigorite (e.g. reviews of Ulmer and Trommsdorff 1999 and Reynar 2013).

According to experiments (Ulmer and Trommsdorff 1995, 1999; Wunder and Schreyer 1997; Bromiley and Pawley 2003; Perrillat et al. 2005; Padrón-Navarta et al. 2010; Maurice et al. 2020), the antigorite decomposition to anhydrous assemblage 'forsterite (Fo) + enstatite (En)' occurs within 600-700 oC at 1-4 GPa. Within this *T* range, the appearance of the intermediate assemblages 'forsterite + talc-like phase' or 'chlorite + olivine + orthopyroxene' is identified in the *in-situ* and quench experiments (Perrillat et al. 2005; Maurice et al. 2020). Among the main factors that thermally stabilize Atg are the elevated Al content in the mineral and high H_2O activity provided by the presence of excess water (Bromiley and Pawley 2003; Perrillat et al. 2005; Padrón-Navarta et al. 2010).

The H_2O activity (aH_2O), as a major factor regulating the dehydration reactions, seems to be indeed critical for the serpentine stability in metamorphic processes. An indicative example is

given by Perrillat et al. (2005) who report the decrease of the antigorite dehydration temperature by 50–100 °C under H_2O-unsaturated conditions at pressure relevant to subduction zone. This effect can be more dramatic upon the further decrease of the aH_2O in the presence of alkali chlorides due to strong non-ideality of saline aqueous fluids at high pressure (Aranovich and Newton 1996, 1997; Mantegazzi et al. 2013). For example, the temperature of 'brucite $Mg(OH)_2$ - periclase MgO' equilibrium is lowered by about 200 °C due to the presence of saturated NaCl aqueous fluid at 1.5-2 GPa (Aranovich & Newton, 1996). Our recent experiments on chrysotile show a ≈ 170 °C low-temperature shift of dehydration reaction in the NaCl-saturated conditions, compared to the H_2O-saturated salt-free system, at 2-4 GPa (Likhacheva et al. 2021). Regarding antigorite, the calculations based on empirical equation of state for the NaCl-H_2O fluid predict the suppression of the dehydration temperature by about 70 °C at 2-3 GPa even in the relatively diluted NaCl-H_2O solution (Mantegazzi et al. 2013).

Alkali-chloride-rich fluid inclusions are abundant in minerals of the mantle wedge rocks and, particularly, in serpentinites (Scambelluri and Philippot 2001; Sharp and Barnes 2004; Kendrick et al. 2017), thus making important the influence of the dissolved salts onto the serpentine stability through the decrease of the H_2O activity. This is especially important for the metamorphic processes in subduction zones, where the localization of dehydration reactions can be sensitive to the temperature shift caused by the presence of aqueous-saline fluids. The aim of this work is to explore the temperature effect of the dissolved salt on the antigorite dehydration at H*P*-H*T* conditions relevant to subduction zone. We present the results of the *in-situ* X-ray diffraction study of the antigorite decomposition at 1.5-3 GPa and 500-700 °C in the presence of NaCl-saturated aqueous fluid; such conditions provide the minimal aH_2O (e.g. Aranovich and Newton 1997) and, thus, would correspond to the maximal temperature shift of the dehydration reaction.

EXPERIMENTAL

We used natural antigorite with the composition $Mg_{2.36}Fe_{0.48}Al_{0.08}Si_{2.00}O_5(OH)_{3.84}$ (by microprobe analysis) from the serpentinites of the Saranovskoe deposit (Ural, Russia). The Raman spectrum of the sample (Fig. 1a) contains several intense bands matching the antigorite spectrum reported by Auzende et al. (2004). The X-ray diffraction pattern (Fig. 1b) could be fitted using the structure model of monoclinic (*C*2/*m*) antigorite polysome with m=16 (Capitani and Mellini 2006); the resulting parameters of the unit cell are a = 87.32(6), b = 9.29(1), c = 7.30(1) Å, β = 91.7(1) °. Though spectroscopic and diffraction data do not reveal mineral admixtures, a slightly elevated sum of octahedral cations (2.92 instead of 2.79-2.87 characteristic of pure antigorite, Mellini et al. 1987), suggests a minor presence of Mg-rich component, possibly chlorite.

A diamond anvil cell (DAC) with gas membrane and resistive heating (graphite heater) was used for *in situ* X-ray diffraction measurements. Powdered antigorite, mixed with NaCl-saturated water solution and solid NaCl, was placed in an 80 μm-diameter hole drilled in the gold insert in the rhenium gasket (outer diameter of the insert is about 150 μm). This insert was necessary to protect the rhenium gasket from corrosion by the fluid caused by enhanced solubility of Mg silicates under pressure (Okada et al. 2002). Solid salt was added to ensure NaCl saturation of supercritical fluid in the H*P*-H*T* experiment. Two reference experiments were performed on antigorite without medium. All samples contained also Au^0 spheres for pressure measurement. The experimental conditions are listed in Table 1. The DAC was heated stepwise from 100 °C to 700 °C and was kept at each temperature step for 0.5-1 h at T > 500 °C, when the decomposition started. The temperature was measured by two R-type thermocouples plunged in insulating glue and contacting the side facets of diamond culets. The temperature in the working chamber (T^{o}_{sample}) was calibrated against the mean value of the thermocouple readings ($T^{o}_{thermocouple}$) with the accuracy of 50 °C using the PVT equations of state of NaCl and Au^0 (Dorogokupets and Dewaele 2007; Fei et al. 2007), whose peaks were present in almost all the

collected diffraction patterns. Such cross calibration is based on the determination of the unit cell volume and construction of the iso-volume lines for NaCl and Au^0 in *P*-*T* diagram (Fig.1Sa). The average coefficient $A = 0.87$ of linear dependences $T^{o}_{sample} = A*T^{o}_{thermocouple}$ (Fig. 1Sb) was used to re-calculate the mean $T^{o}_{thermocouple}$ values throughout all the runs.

The X-ray powder diffraction measurements were performed at the Extreme Conditions Beamline P02.2 of PETRA III (Hamburg, Germany), at a wavelength of 0.2898 Å and a beam size of 8×3 μm (Liermann et al. 2015). Diffraction patterns were collected using a PE XRD1621 flat-panel detector and integrated with the program DIOPTAS 0.5.1 (Prescher and Prakapenka 2015). CeO_2 was used to calibrate the instrumental parameters.

RESULTS

Antigorite decomposition in the NaCl-free dry conditions

The diffraction patterns of antigorite collected on the *P*, *T* increase are shown in Fig. 2 (run # 2d). At 2.5 GPa, antigorite is stable up to 700 ^{o}C. This result is reproduced in the run # 1d (diffraction data are not shown) where no signs of the reaction were observed up to 690^{o}C. At 720^{o}C, the Atg peaks gradually decrease along with the growth of the peaks assigned to newly formed forsterite. Additional new peaks at $2\Theta = 5.02, 8.17, 10.83, 11.05$ ^{o} are characteristic of a high-pressure phyllosilicate 10 Å phase (Fumagalli et al. 2001). The *P* value of this run (2.5 GPa) is slightly lower than the boundary between talc (Tlc) and the 10 Å phase (Pawley and Wood 1995). Nevertheless, taking into account the absence of the intense Tlc reflection at about 5.34 ^{o} (d = 3.11 Å) (Gatta et al. 2013), the assignment of the above new peaks to the 10 Å phase seems more appropriate. The observation of the intermediate products of the antigorite decomposition agrees with the data by Perrillat et al. (2005).

Antigorite decomposition in the presence of NaCl

The H*P*-H*T* diffraction patterns collected on antigorite mixed with the NaCl-H_2O fluid (runs # 1s-3s, Table 1) are presented in Figs. 3-5. The presence of the NaCl reflections in diffraction patterns demonstrates that the fluid was NaCl-saturated in all runs (see also footnotes to Table 1).

At about 2 GPa (run # 1s), antigorite becomes unstable at temperature as low as 540 ^{o}C. It is manifested by the decrease and broadening of its diffraction peaks (Fig. 3). New peaks of talc appear simultaneously. Their rapid growth along with the forsterite peaks proceeds on the further temperature increase up to 640 ^{o}C. Above 2 GPa, the Atg degradation begins at a slightly higher temperature (runs # 2s, 3s, Figs. 4,5). The temperature of 580-590 ^{o}C, when the Atg peaks almost disappear, surely marks the highest limit for the decomposition onset, whereas the equilibrium must be at a lower temperature in the range of 550-570 ^{o}C. Interestingly, in the runs # 2s and 3s, which contained higher proportion of the fluid than the run # 1s, no or only minor peaks of the product phases appear along with the decrease of the Atg peaks. Tlc appears in the range of 590-630 ^{o}C (Fig. 5), whereas Fo and En are present at higher temperature only. The thermal delay between the formation of the intermediate (Tlc+Fo) and final assemblages (Fo+En) is similar to that found in the kinetic experiments of Perrillat et al. (2005). The Fo peaks disappear along with those of Tlc on heating from 630 to 650 ^{o}C (Fig. 5). This feature may be a sign of dissolution of the product Mg silicates in the fluid (see below).

Thus, similarly to the salt-free conditions (run #2d), the intermediate products of the Atg decomposition (Tlc+Fo) appear first in the presence of the NaCl-H_2O fluid. These first signs of the reaction, along with the Atg degradation, apparently mark the dehydration temperature (T^{o}_{deh}) more properly, than the final anhydrous phases, because there is possible overstepping of equilibrium in short-term experiments. At 1.5-3 GPa, the T^{o}_{deh} is in the range of 540-570 ^{o}C in the presence of the NaCl-H_2O fluid, whereas the minimal temperature of the Atg degradation is 700 ^{o}C in the NaCl-free system (run #2d, Fig. 2). Therefore, there is a definite shift of the Atg

157 dehydration by about 150 °C to lower temperature in the presence of the NaCl-bearing fluid,
158 compared to the salt-free dry conditions.
159
160 **DISCUSSION**
161 Figure 6 compares the *P-T* position of the Atg dehydration reaction, roughly bracketed by the
162 presented experiments, in the salt-bearing and salt-free system. The reaction temperature in the
163 salt-free dry system (700 °C at 2 GPa) is similar to that found in the equilibrium experiments on
164 the H_2O-saturated systems (Ulmer and Trommsdorff 1999). Taking into account the difference
165 between the T^{o}_{deh} in the H_2O-saturated and non-saturated system observed earlier (Perrillat et al.
166 2005), for the water-saturated conditions of our short-term experiments the maximal T^{o}_{deh} can be
167 estimated no less than 750 °C at 2 GPa. Accordingly, the maximal low-temperature shift of the
168 reaction due to the presence of saturated NaCl-H_2O fluid can be estimated as 200 °C.
169 Since the H_2O activity is the major factor controlling the T^{o}_{deh}, the observed difference
170 indicates the lowest $a$$H_2O$, provided by the lowest X_{H2O} in the salt-saturated NaCl-H_2O fluid. The
171 calculations, based on the experimentally obtained densities of the NaCl–H_2O fluids (Mantegazzi
172 et al. 2013), predict the suppression of T^{o}_{deh} by 60 °C when the molar portion of water in the
173 fluid X_{H2O} decreases from 1 to ≈ 0.95 at 2.5 GPa (thin dashed curves in Fig. 6). Based on this
174 calculation and the estimated ΔT^{o}_{deh} = 200 °C, we infer that at 2-3 GPa / 550-600 °C halite
175 saturation is achieved at X_{H2O} ≈ 0.85. This fits to the NaCl solubility at 2-4 GPa and 600-700 °C
176 which can be roughly extrapolated from the data of Aranovich and Newton (1996) for 0.2-1.5
177 GPa and 600-900 °C.
178 Notably, pressure has opposite effect on the NaCl solubility and aNaCl (at a certain
179 X_{H2O}): the first decreases and the second increases with pressure (Mantegazzi et al. 2013).
180 Accordingly, these two effects (the decrease of the NaCl solubility and growth of aNaCl at a
181 fixed X_{H2O}) make opposite contribution to the resulting aNaCl (and $a$$H_2O$). The second effect
182 (growth of aNaCl at a fixed X_{H2O}) manifests in a larger deviation of calculated T^{o}_{deh} with

pressure: the thin dashed lines in Fig. 6 calculated for ideal and non-ideal NaCl-H_2O mixing at X_{H2O} = 0.949 diverge, and the reaction slope becomes negative above 2 GPa. On the other hand, our experimental (thick solid) curve for saturated NaCl-H_2O fluid has sub-vertical or even slightly positive slope. Apparently, this is a consequence of a stronger effect of the decrease of NaCl solubility (and *a*NaCl) with pressure, in agreement with the dependences aH_2O/X_{H2O} for various pressures presented in Fig. 10 of the paper of Mantegazzi et al. (2013). Based on these dependences, the aH_2O of the NaCl-H_2O fluid saturated at $X_{H2O} \approx 0.85$ ($X_{NaCl} \approx 0.15$) can be estimated as ≈ 0.4.

Typical NaCl concentrations of the fluids derived from the deep subduction/upper mantle sources vary from 5 to 20 wt.% (up to $X_{NaCl} \approx 0.08$). However, many fluid inclusions in H*P* metamorphic rocks show salinities as high as 30-50 wt.% ($X_{NaCl} \approx 0.1$-0.2) (Phillippot et al. 1995, 1998; Kendrick et al. 2017). Such extreme chloride enrichment is generally interpreted as a result of water escape from the inclusions during the retrograde *P*-*T* evolution (Frezzotti and Ferrando 2015). Indeed, a complex history of deep subduction fluids, including devolatilization and metasomatic reactions at H*P* conditions, often obscures their primary composition. Concerning chlorine content in serpentine minerals, it is shown that during the prograde metamorphic lizardite/antigorite transition more than 50% of the Cl is removed from serpentine (Debret et al. 2014). But still, this loss is far from a total removal. Besides, the bulk rock analyses, for example, of sea-floor serpentinites, show high Cl contents (above 0.5 wt.% Cl); this promoted a model for the generation of high-salinity fluids via the breakdown of subducted serpentinites bearing large amounts of seawater components (Sharp and Barnes 2004). The mentioned lizardite/antigorite transition can contribute to the generation of such deep saline fluids. Taking into account the uncertainty over the rocks permeability and associated fluid circulation in subducting slab (Ferrand 2019), an active interaction between the salt-enriched fluids and serpentine cannot be ruled out.

208 The absence or only minor presence of crystalline products of the Atg decomposition at
209 actual H*P*-H*T* conditions in the NaCl-bearing runs # 2s, 3s (Figs. 4, 5) demands a special
210 attention. Indicative feature is the appearance of the minor Fo peaks at 630 ^{o}C and their
211 subsequent disappearance at 650 ^{o}C (run # 3s, Fig. 5). In both these runs, the proportion of a
212 fluid was high. Notably, in the run # 2d without fluid and the run # 1s with minor proportion of
213 the fluid, Fo and Tlc/10 Å phase readily crystallize at H*P*-H*T* conditions (Figs. 2, 3). This clearly
214 indicates a complete or partial dissolution of the product Mg silicates, if a sufficient amount of
215 the fluid phase is available. The presence of NaCl in the fluid is critical. The *in situ* studies of
216 Atg decomposition using pure H_2O do not report appreciable dissolution of the reaction
217 products. For example, in the runs with 20 wt.% of H_2O forsterite formed readily along with the
218 talc-like phase at 1-5 GPa and 550-700 ^{o}C (Perrillat et al. 2005). Enhanced solubility of Mg-
219 silicates in the NaCl-H_2O solutions is demonstrated by Macris et al. (2020). At 1 GPa, 800 and
220 900 ^{o}C, the Fo solubility in pure H_2O is low, but it increases greatly with rising NaCl
221 concentration in the fluid. The relation between the increase of the NaCl activity and the degree
222 of dissociation of solute NaCl in the concentrated aqueous fluid at $P > 1$ GPa, which explains its
223 enhanced solvent properties, was first discussed by Aranovich and Newton (1996, 1997).
224 Another example of enhanced solubility of the reaction products in concentrated NaCl-H_2O fluid
225 is given by our data on chrysotile (Likhacheva et al. 2021): at 2-4 GPa and 380 ^{o}C Tlc/Tlc-like
226 phase only crystallizes as product of the reaction "chrysotile → Fo + Tlc", whereas Fo appears
227 after the *P*,*T* release. In the diffraction patterns collected during the Atg decomposition at the
228 highest experimental temperatures, the En peaks are prevalent (Figs. 4, 5). This observation
229 agrees with a lower En solubility in the concentrated NaCl-H_2O fluid, compared to Fo (Macris et
230 al. 2020). In addition, our data on antigorite and chrysotile indicate that the range of high Fo
231 solubility expands to lower temperatures (< 700 ^{o}C) with the pressure increase above 1 GPa.
232
233

IMPLICATIONS

The present data provide a first experimental evidence for a significant shift of the antigorite dehydration reaction to lower temperature due to the lowering of the water activity in concentrated NaCl-H_2O fluid. The maximum possible temperature shift in the NaCl-saturated fluid, compared to the salt-free H_2O-saturated system, is estimated at around –200 ^oC at 1.5-3 GPa. Although high-pressure metamorphic fluids are typically far from salt saturation, the existence of high-salinity (and low-$a$$H_2O$) fluids at the H$P$-H$T$ conditions cannot be excluded. Therefore, the corresponding decrease of dehydration temperature in the presence of alkali-chlorides can be significant. This is especially critical for serpentinites in subducting slab passing the area beneath the volcanic arc with the highest thermal gradients. The present experimental data also support the model of Sharp and Barnes (2004) who suggested an extension of the *P*-*T* area of serpentinite dehydration in subducting slab due to the reaction shift to lower temperatures in the presence of the concentrated chloride-bearing aqueous fluid. In particular, the decrease of T^o_{deh} by 200 ^oC implies the raise of the reaction location by about 20 km for a normal subduction geotherm, or more for the critical point beneath the volcanic arc. Such spreading of the reaction boundaries helps to explain the broad seismic zone of intermediate-level earthquakes that are attributed to serpentine dehydration.

The example of antigorite dehydration also demonstrates active dissolution of Mg silicates, first of all, forsterite, in the NaCl-H_2O fluid at 600-700 ^oC and 1.5-3 GPa. Thus, the serpentine dehydration contributes to the formation of MgO and SiO2-enriched fluids, which are important agents of deep metasomatic processes in the mantle wedge.

Acknowledgements and Funding. We thank Prof. E. M. Spiridonov (Moscow State University) for providing us with the antigorite sample. The authors acknowledge DESY (Hamburg, Germany), a member of the Helmholtz Association HGF, for the provision of experimental facilities. This work is performed on state assignment of IGM SB RAS and is supported by the

RFBR project # 18-05-00312. Diffraction experiments were carried at the DESY PETRA III research laboratory and supported by the approval of PETRA III regular proposal I-20190140.

REFERENCES CITED

Aranovich, L.Ya., and Newton, R.C. (1996) H_2O activity in concentrated NaCl solutions at high pressures and temperatures measured by the brucite-periclase equilibrium. Contributions to Mineralogy and Petrology, 125, 200–212.

Aranovich, L.Ya., and Newton, R.C. (1997) H_2O activity in concentrated KCl and KCl-NaCl solutions at high temperatures and pressures measured by the brucite-periclase equilibrium. Contributions to Mineralogy and Petrology, 127, 261–271.

Auzende, A.-L., Daniel, I., Reynard, B., Lemaire, C., Guyot, F. (2004) High-pressure behavior of serpentine minerals: a Raman spectroscopic study. American Mineralogist, 31, 269–277.

Bromiley, G.D., and Pawley, A.R. (2003) The stability of antigorite in the systems MgO-SiO_2-H_2O (MSH) and MgO-Al_2O_3-SiO_2-H_2O (MASH): The effects of Al^{3+}substitution on high-pressure stability. American Mineralogist, 88, 99–108.

Capitani, G.C., and Mellini, M. (2006) The crystal structure of a second antigorite polysome (m = 16), by single-crystal synchrotron diffraction. American Mineralogist, 91, 394-399.

Debret, B., Koga, K.T., Nicollet, C., Andreani M., Schwartz, S. (2014) Cl and S input via serpentinite in subduction zones: implications for the nature of the fluid released at depth. Terra Nova, 26, 96–101.

Dorogokupets, P.I., and Dewaele, A. (2007) Equations of state of MgO, Au, Pt, NaCl-B1, and NaCl-B2: Internally consistent high-temperature pressure scales. High Pressure Research. 27:4, 431–446.

Fei, Y., Ricolleau, A., Frank, M., Mibe, K., Shen, G., Prakapenka, V. (2007) Toward an internally consistent pressure scale. PNAS, 104, 9182–9186.

Ferrand, T.P. (2019) Neither antigorite nor its dehydration is “metastable”. American mineralogist, 104, 788-790.

Frezzotti, M.L., and Ferrando, S. (2015) The chemical behavior of fluids released during deep subduction based on fluid inclusions. American Mineralogist, 100, 352–377.

Fumagalli, P., Stixrude, L,. Poli, S., Snyder, D. (2001) The 10A phase: a high-pressure expandable sheet silicate stable during subduction of hydrated lithosphere. Earth and Planetary Science Letters, 186, 125–141.

Gatta, G.D., Merlini, M., Valdre, G., Liermann, H.-P., Nenert, G., Rothkirch, A., Kahlenberg, V., Pavese, A. (2013) On the crystal structure and compressional behaviour of talc: a mineral of interest in petrology and material science. Physics and Chemistry of Minerals, 40, 145–156.

Kendrick, M.A., Hémond, C., Kamenetsky, V.S., Danyushevsky, L., Devey, C.W., Rodemann, T., Perfit, M. (2017) Seawater cycled throughout Earth's mantle in partially serpentinized lithosphere. Nature Geosciences, 10, 222–228.

Liermann, H.-P., Konopkova, Z., Morgenroth, W., Glazyrin, K., Bednarcik, J., McBride, E. E., et al. (2015) The extreme conditions Beamline P02.2 and the extreme conditions science infrastructure at PETRA III. Journal of Synchrotron Radiation, 22(4), 908–924.

Likhacheva, A..Yu., Goryainov, S.V., Rashchenko, S.V., Dementiev, S.N., Safonov O.G. (2021) In situ observation of chrysotile decomposition in the presence of NaCl-bearing aqueous fluid up to 5 GPa and 400 ^{o}C. Mineralogy and Petrology, 115, 213–222.

Macris, C.A., Newton, R.C., Wykes, J., Pan, R., Manning, C.E. (2020) Diopside, enstatite and forsterite solubilities in H_2O and H_2O-NaCl solutions at lower crustal and upper mantle conditions. Geochimica and Cosmochimica Acta, 279, 119–142.

Mantegazzi, D., Sanchez-Valle, C., Driesner, T. (2013) Thermodynamic properties of aqueous NaCl solutions to 1073 K and 4.5 GPa, and implications for dehydration reactions in subducting slabs. Geochimica and Cosmochimica Acta, 121, 263–290.

Maurice, J., Bolfan-Casanova, N., Demouchy, S., Chauvigne, P., Schiavi, F., Debret, B. (2020) The intrinsic nature of antigorite breakdown at 3 GPa: Experimental constraints on redox conditions of serpentinite dehydration in subduction zones. Contributions to Mineralogy and Petrology, 175, 94.

Mellini, M. (1982) The crystal-structure of lizardite-1T: hydrogen bonds and polytypism. American Mineralogist, 67, 587–598.

Mellini, M., Trommsdorff, V., Compagnoni, R. (1987) Antigorite polysomatism: behaviour during progressive metamorphism. Contributions to Mineralogy and Petrology, 97, 147–155.

Okada, T., Utsumi, W., Kaneko, H., Yamakata, M., Shimomura, O. (2002) In situ X-ray observations of the decomposition of brucite and the graphite–diamond conversion in aqueous fluid at high pressure and temperature. Physics and Chemistry of Minerals, 29, 439–445.

Padrón-Navarta, J.A., Hermann, J., Garrido, C.J., López Sánchez-Vizcaíno, V., Gómez-Pugnaire, M.T. (2010) An experimental investigation of antigorite dehydration in natural silica-enriched serpentinite. Contributions to Mineralogy and Petrology, 159, 25–42.

Pawley, A.R., and Wood, B.J. (1995) The high-pressure stability of talc and 10Å phase: potential storage sites for H_2O in subduction zones. American Mineralogist, 89, 998-1003.

Perillat, J.P., Daniel, I., Koga, K.T., Reynard, B., Cardon, H., Crichton, W.A. (2005) Kinetics of antigorite dehydration: A real time X-ray study. Earth and Planetary Science Letters, 236, 899–913.

Philippot, P., Chevallier, P., Chopin, C., Dubessy, J. (1995) Fluid composition and evolution in coesite-bearing rocks (Dora-Maira massif, Western Alps): Implications for element recycling during subduction. Contributions to Mineralogy and Petrology, 121, 29–44.

Philippot, P., Agrinier, P., Scambelluri, M. (1998) Chlorine cycling during subduction of altered oceanic crust. Earth and Planetary Science Letters, 161, 33–44.

Prescher, C., and Prakapenka, V.B. (2015) DIOPTAS: a program for reduction of two-dimensional X-ray diffraction data and data exploration. High Pressure Research, 35(3), 223–230.

Reynard, B. (2013) Serpentine in active subduction zones. Lithos, 178, 171–185.

Scambelluri, M., and Philippot, P. (2001) Deep fluids in subduction zones. Lithos, 55, 213–227.

Schmidt, M.W., and Poli, S. (1998) Experimentally based water budgets for dehydrating slabs and consequences for arc magma generation. Earth and Planetary Science Letters, 163, 361–379.

Sharp, Z.D., and Barnes, J.D. (2004) Water-soluble chlorides in massive seafloor serpentinites: A source of chloride in subduction zones. Earth and Planetary Science Letters, 226, 243–254.

Toby, B., and Von Dreele, R.B. (2013) GSAS-II: The Genesis of a Modern Open-Source All-Purpose Crystallography Software Package. Journal of Applied Crystallography, 46, 544-549

Ulmer, P., and Trommsdorff, V. (1995) Serpentine stability to mantle depths and subduction-related magmatism. Science, 268(5212), 858–861.

Ulmer, P., and Trommsdorff, V. (1999) Phase relations of hydrous mantle subducting to 300 km. In: Fei , Bertka CM, Mysen BO (eds) Mantle petrology: field observations and high pressure experimentation: a tribute to Francis R. Boyd, Geochemical. Society, Special Publication 6, pp. 259–281.

Wicks, F.J., and Whittaker, E.J.W. (1975) A reappraisal of the structures of the serpentine minerals. Canadian Mineralogist, 13, 227–243.

Wunder, B., and Schreyer, W. (1997) Antigorite: High-pressure stability in the system MgO-SiO_2-H_2O (MSH). Lithos, 41, 213–227.

Zussman, J. (1954) Investigation of the crystal structure of antigorite. Mineralogical Magazine, 30, 498–512.

388 **Figure captions.**

389

390 Fig. 1. Raman spectrum (**a**) and the X-ray diffraction pattern (**b**) of antigorite fitted with
391 m=16 polysome structure (Capitani and Mellini 2006) using GSAS-II (4408) program package
392 (Toby and Von Dreele 2013).

393 Fig. 2. H*P*-H*T* X-ray diffraction patterns of antigorite (run #2d). Initial sample contains
394 small admixture of chondrodite (Chn) which disappears at 700 ^{o}C. *Asterisks* mark the peaks of
395 Re gasket. The peaks of newly formed forsterite (*circles*) and the 10 Å phase (*squares*) are
396 marked. The vertical arrow indicates the run time.

397 Fig.3. H*P*-H*T* X-ray diffraction patterns of antigorite mixed with saturated NaCl-H2O fluid
398 (run #1s). The peaks of newly formed forsterite (*circles*) and talc (*squares*) are marked. The cut-
399 off 2Θ range of 8-9 ^{o} contains strong peaks of Au^0, NaCl, and no intense peaks of the initial and
400 product phases.

401 Fig.4. H*P*-H*T* X-ray diffraction patterns of antigorite mixed with saturated NaCl-H2O fluid
402 (run #2s). The peaks of newly formed enstatite (*triangles*) are marked.

403 Fig.5. H*P*-H*T* X-ray diffraction patterns of antigorite mixed with saturated NaCl-H2O fluid
404 (run #3s). The peaks of newly formed forsterite (*circles*) and enstatite (*triangles*) are marked.
405 The cut-off 2Θ range of 7.5-9 ^{o} contains strong peaks Au^0, NaCl, and no intense peaks of the
406 initial and product phases.

407 Fig. 6. Experimental data points corresponding to Atg preservation (*filled symbols*) and
408 degradation/growth of Fo+Tlc/10 Å phase (*empty symbols*) in the presence of saturated NaCl-
409 H_2O fluid (*squares*) and in H_2O-unsaturated salt-free conditions (*rhombs*). *Thick lines* mark the
410 location of the Atg dehydration reaction in the presence of saturated NaCl-H_2O fluid,
411 corresponding to $X_{H2O} \approx 0.85$ (*black line*) and H_2O-unsaturated salt-free conditions (*grey line*).
412 *Thin solid line* shows the experimental boundary for the Atg dehydration determined by the
413 equilibrium experiments in H_2O-saturated conditions ($aH_2O = 1$) (Ulmer and Trommsdorff

1999). *Thin dashed and dotted lines* mark the calculated reaction boundary at X_{H2O} = 0.949 for non-ideal and ideal mixing between water and NaCl (Mantegazzi et al. 2013). Abbreviations: Atg – antigorite, Fo – forsterite, Tlc – talc/10 Å phase.

Table 1. Experimental data on the antigorite decomposition in the NaCl-H_2O solution (s) and fluid-free dry conditions (d). Abbreviations: Atg - antigorite, Tlc - talc, Fo - forsterite, En - enstatite.

Run #	Starting materials		X_{NaCl}* in fluid	Starting T (°C) / P (GPa)	T (°C) / P (GPa) of Atg degradation	Max T (°C) / P (GPa)	Run products
	crystalline compound	liquid					
1s	Atg, NaCl	saturated NaCl-H_2O solution (X_{NaCl} = 0.1)	sat**	190 / 1.4	540 / 1.5	640 / 1.8	Fo, Tlc
2s	Atg, NaCl	– // –	sat	100 / 1.5	560-580 / 3.0	690 / 2.3	minor En
3s	Atg, NaCl	– // –	sat	100 / 2.8	550-590 / 2.6	670 / 2.7	minor En
1d	Atg	–	0	190 / 0.5	–	690 / 1.8	Atg
2d	Atg	–	0	260 / 1.0	700 / 2.3	720 / 2.5	Atg, Fo, 10 Å phase

*Molar fraction of NaCl, mole NaCl/(NaCl+H_2O). Halite saturation curves in the system NaCl-H_2O (Koster Van Groos 1991) extrapolated to 1 GPa by Aranovich & Newton (1996) allow rough estimation of the saturation X_{NaCl} at our experimental P-T conditions at ≈ 0.15.

Figure 1a

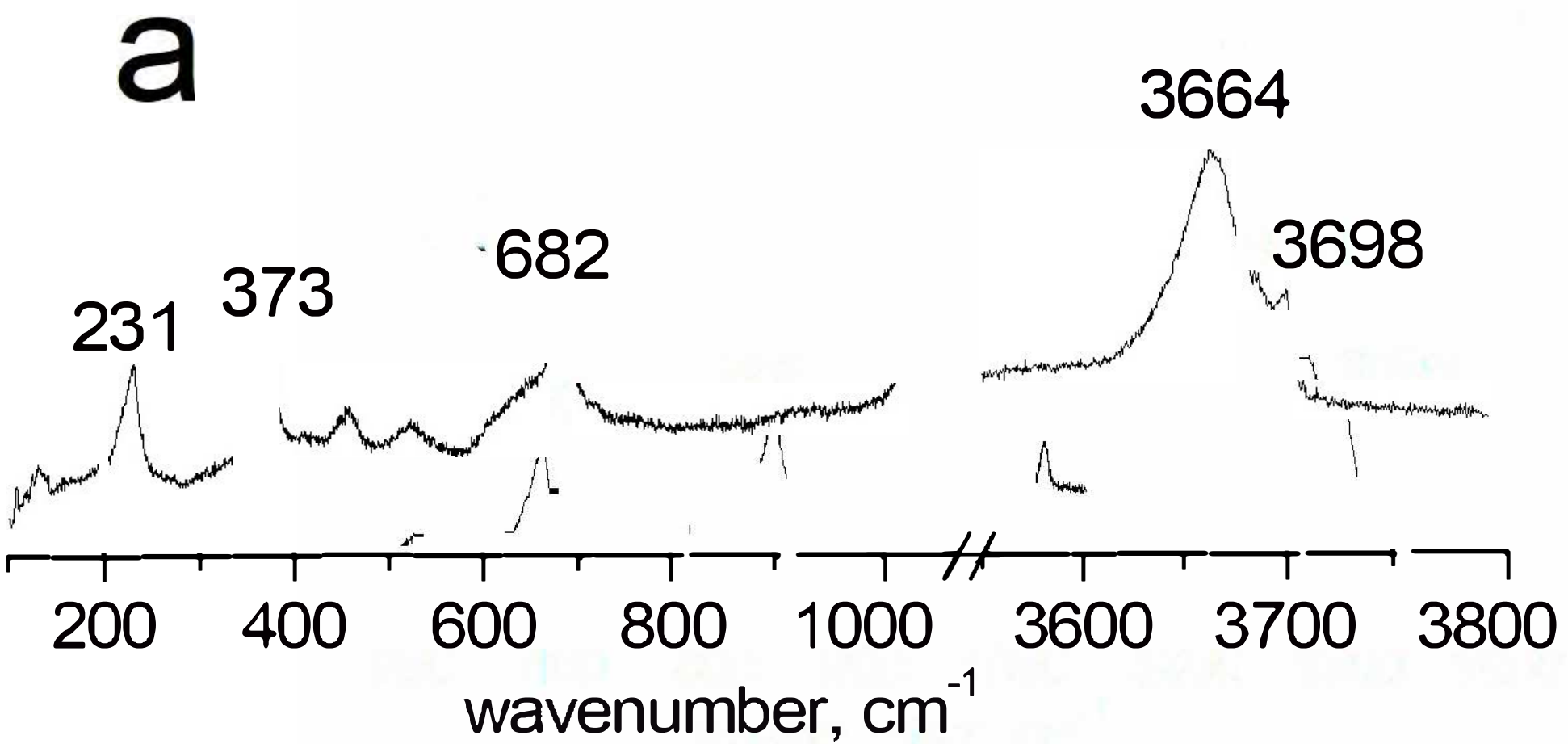
a
231
373
682
3664
3698
200
400
600
800
1000
3600
3700
3800
wavenumber, cm-1

Figure 1b

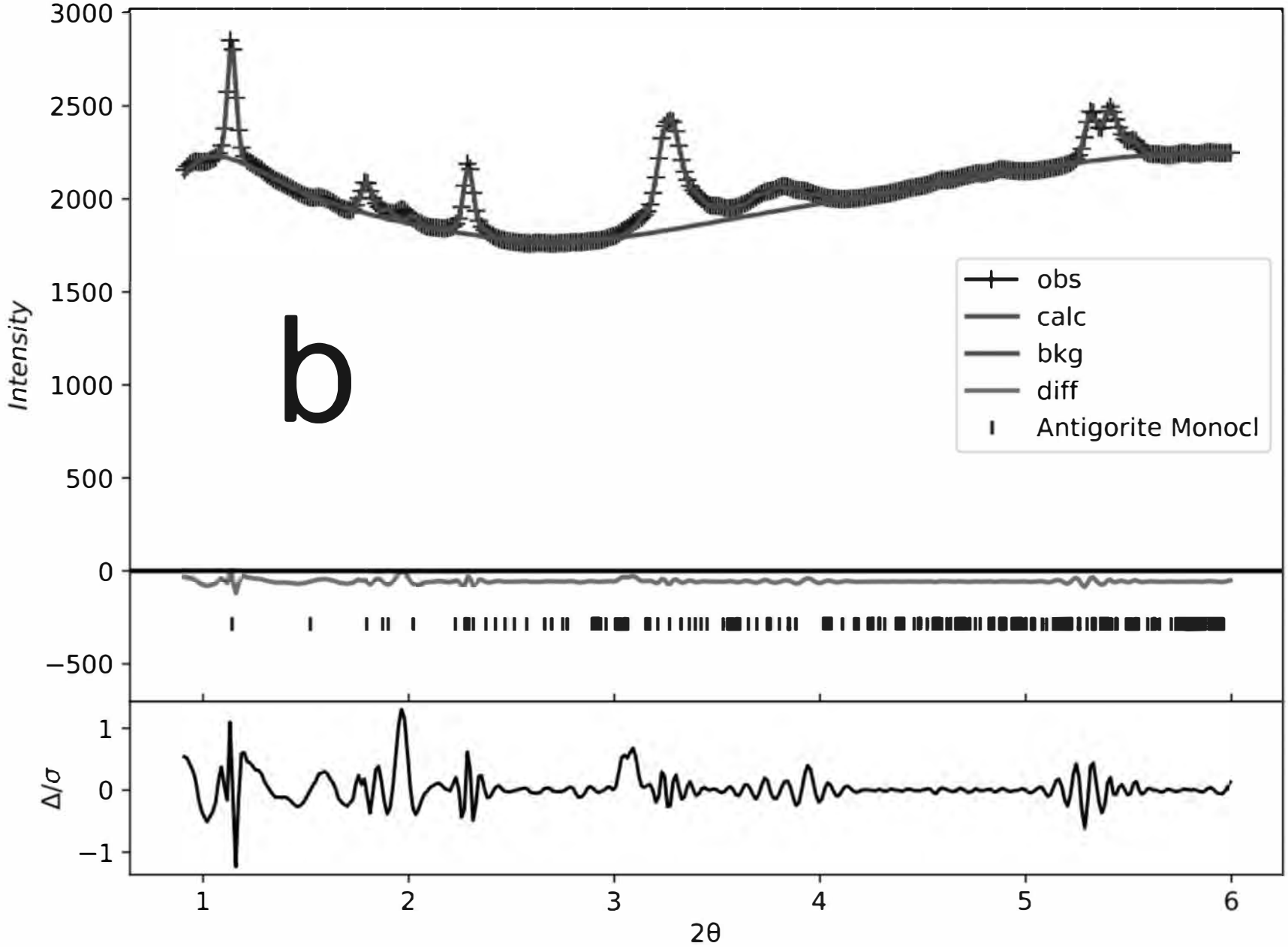
b
obs
calc
bkg
diff
Antigorite Monocl
Intensity
3000
2500
2000
1500
1000
500
0
−500
Δ/σ
1
0
−1
1
2
3
4
5
6
2θ

Figure 2

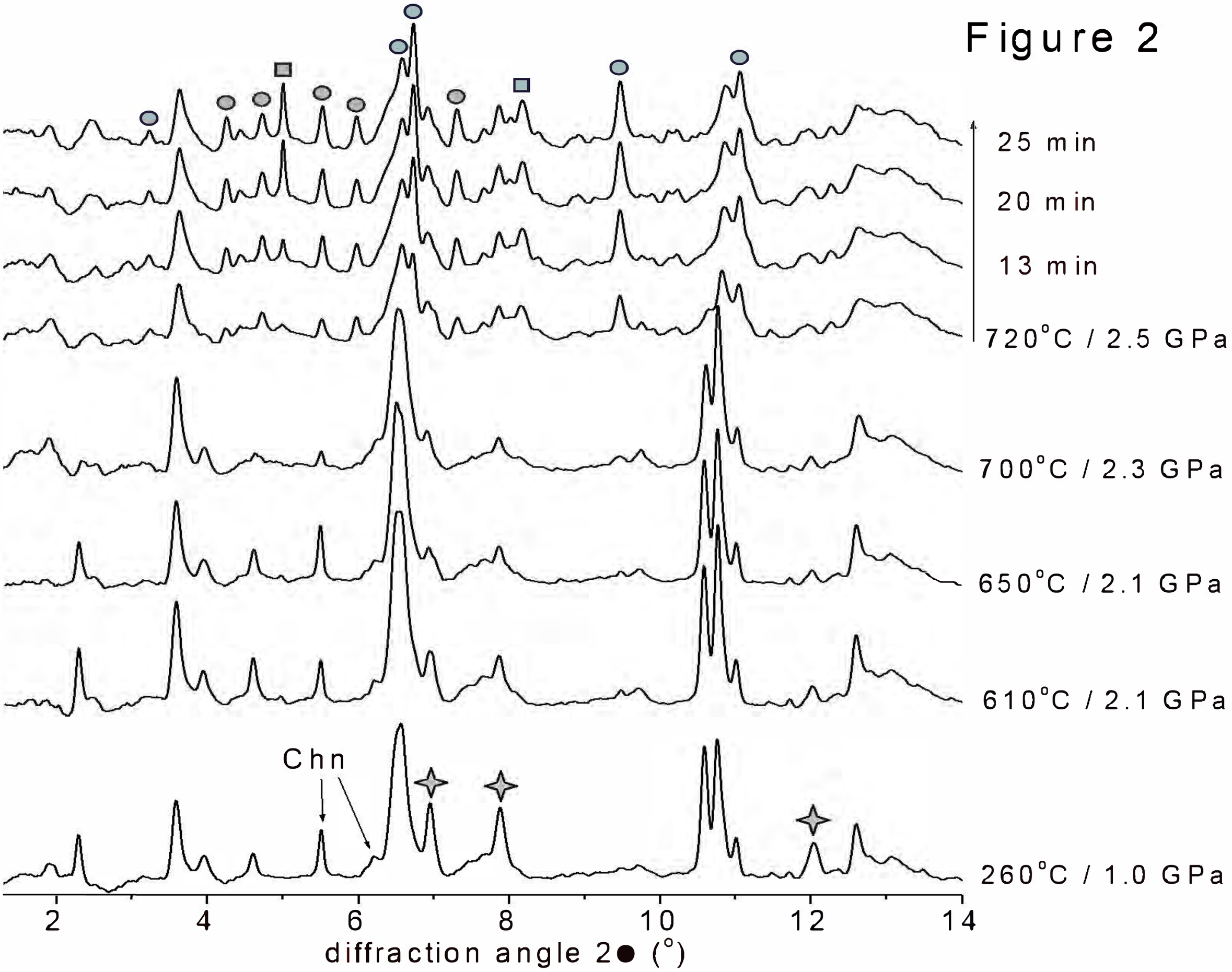
25 min
20 min
13 min
720°C / 2.5 GPa
700°C / 2.3 GPa
650°C / 2.1 GPa
610°C / 2.1 GPa
Chn
260°C / 1.0 GPa
2
4
6
8
10
12
14
diffraction angle 2● (°)

Figure 3

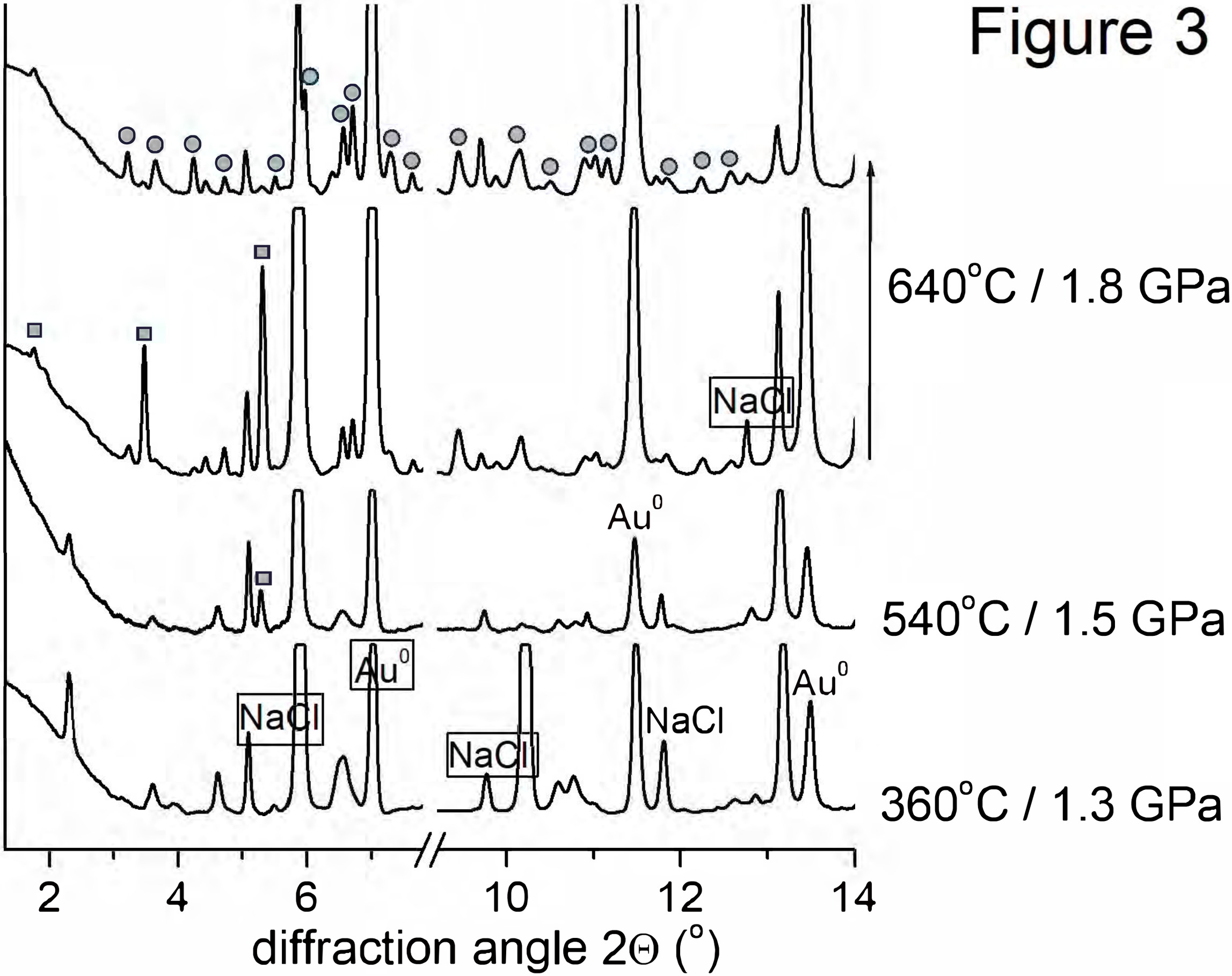
NaCl
640°C / 1.8 GPa
Au0
540°C / 1.5 GPa
NaCl
Au0
NaCl
NaCl
Au0
360°C / 1.3 GPa
2
4
6
10
12
14
diffraction angle 2Θ (°)

Figure 4

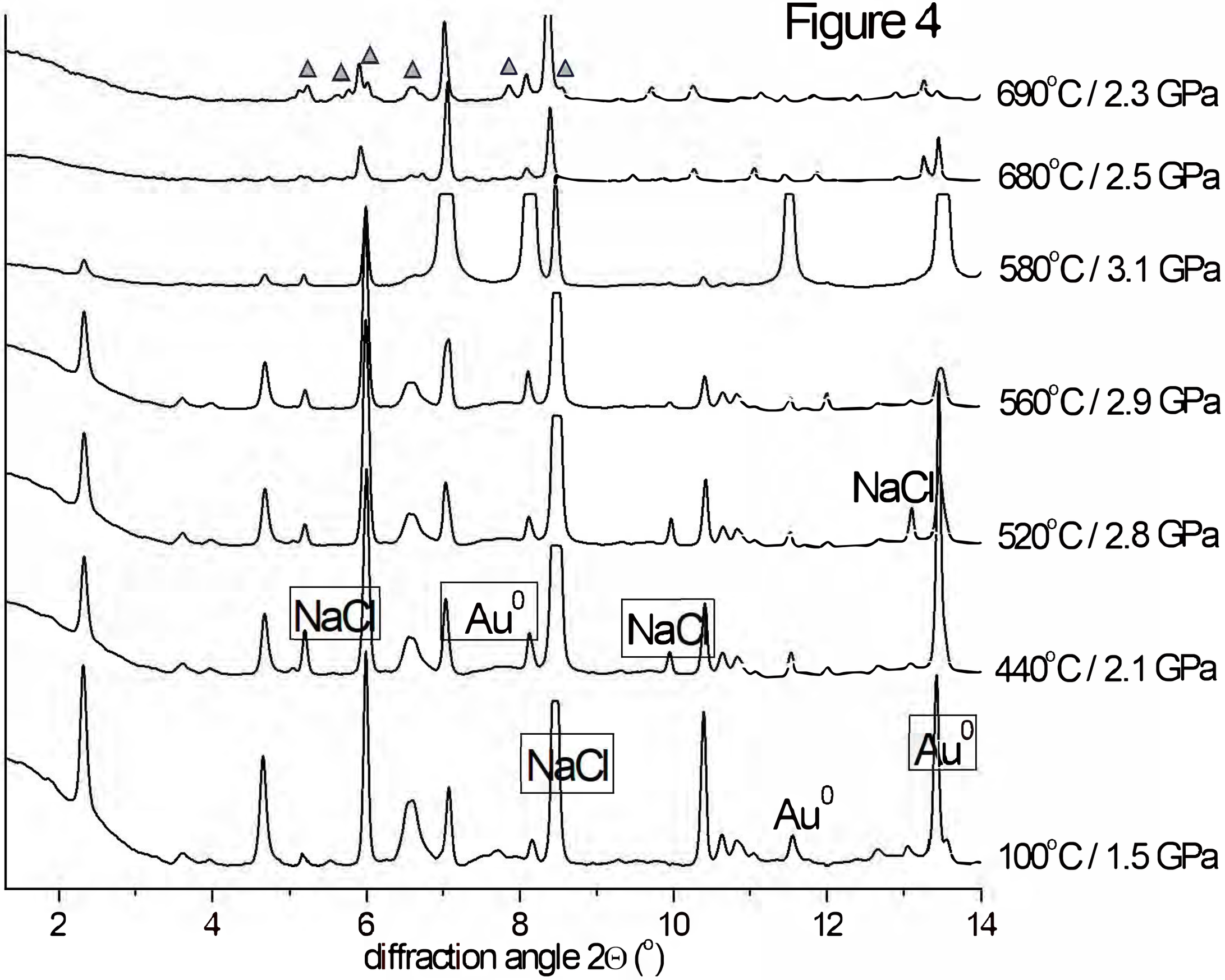
690°C / 2.3 GPa
680°C / 2.5 GPa
580°C / 3.1 GPa
560°C / 2.9 GPa
520°C / 2.8 GPa
440°C / 2.1 GPa
100°C / 1.5 GPa
NaCl
Au0
NaCl
NaCl
Au0
NaCl
Au0
2
4
6
8
10
12
14
diffraction angle 2Θ (°)

Figure 5

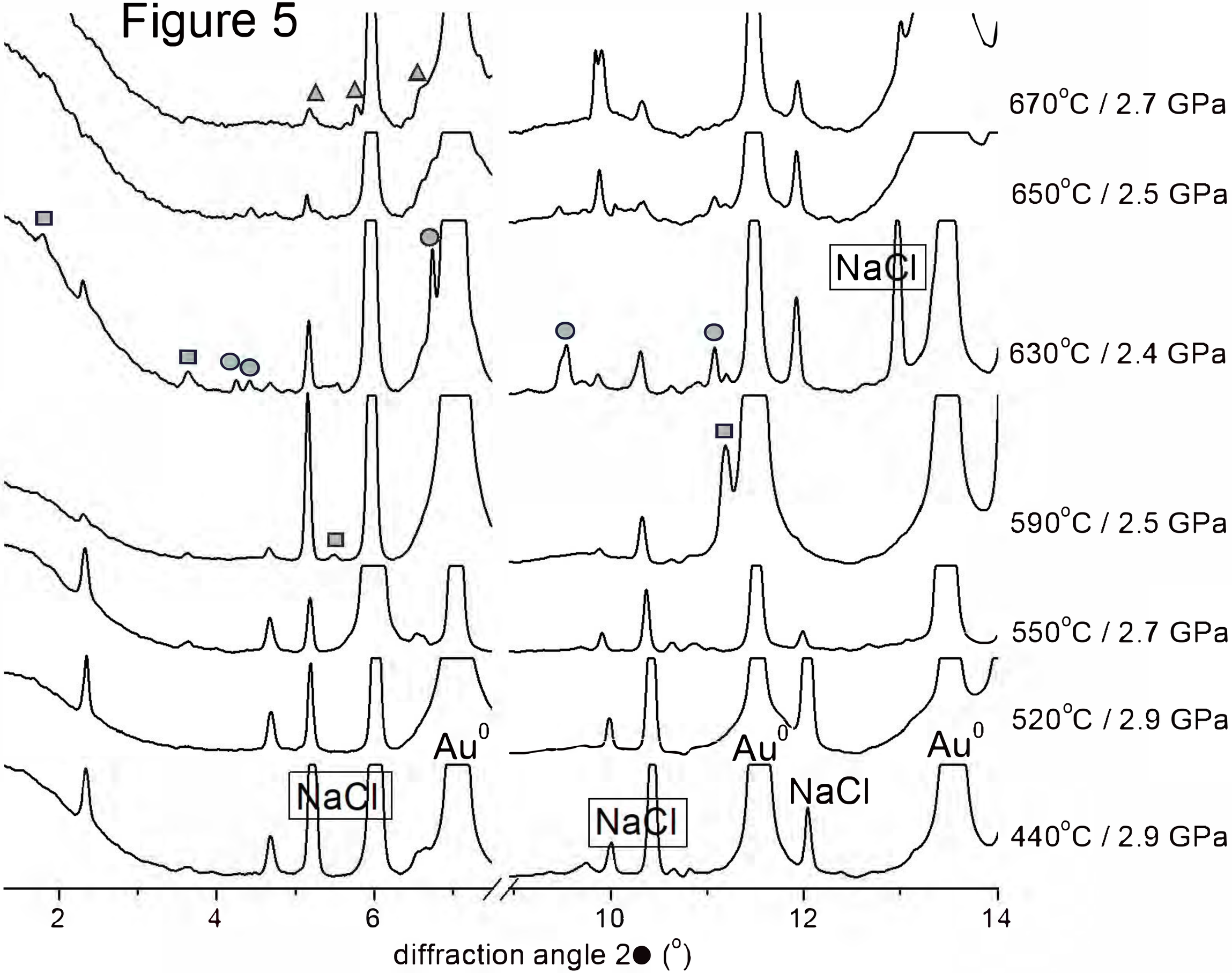
670°C / 2.7 GPa
650°C / 2.5 GPa
NaCl
630°C / 2.4 GPa
590°C / 2.5 GPa
550°C / 2.7 GPa
520°C / 2.9 GPa
Au0
NaCl
NaCl
Au0
Au0
NaCl
440°C / 2.9 GPa
2
4
6
10
12
14
diffraction angle 2● (°)

Figure 6

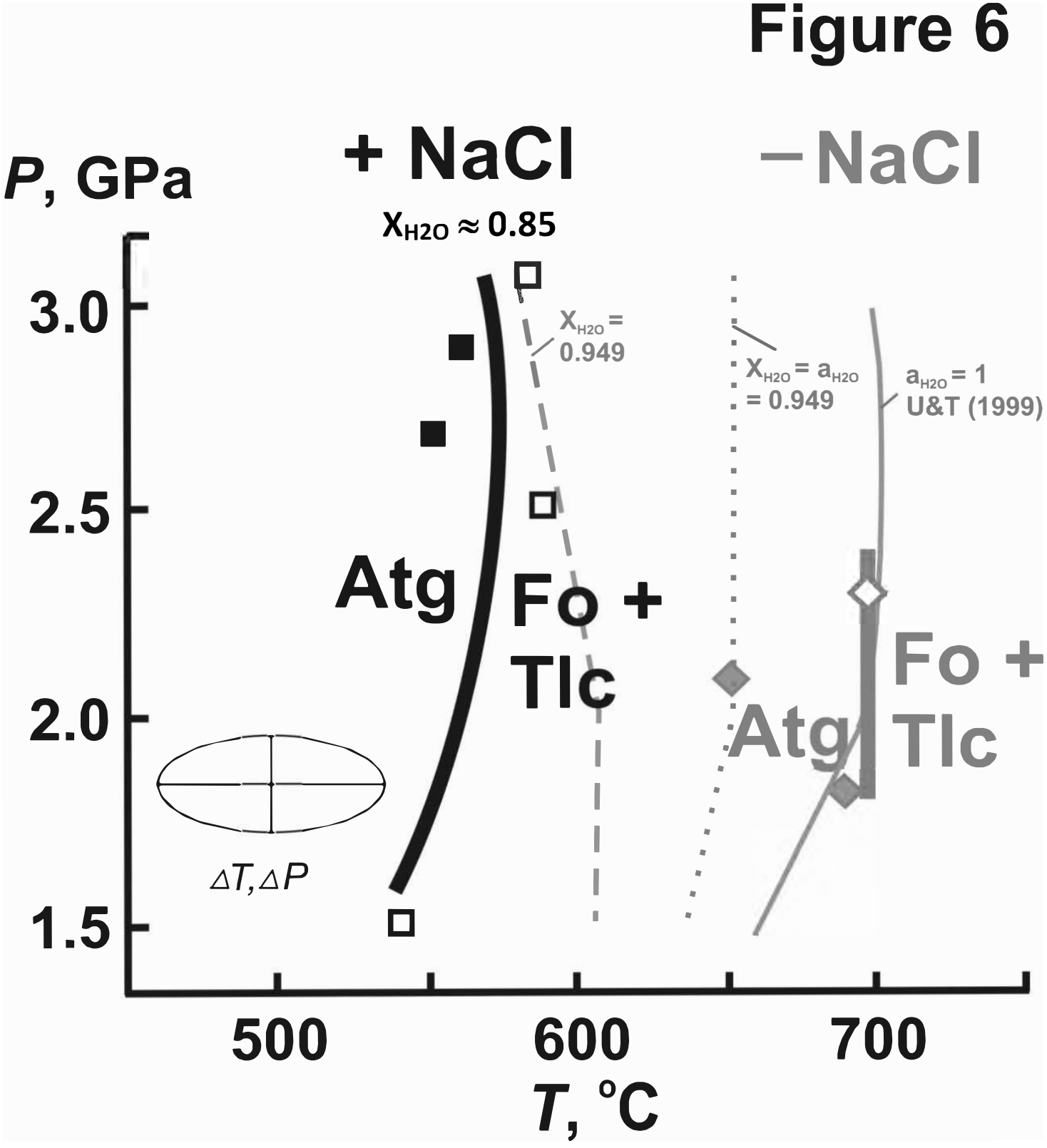
+ NaCl
$X_{H2O} \approx 0.85$
− NaCl
P, GPa
3.0
2.5
2.0
1.5
X_{H2O} = 0.949
$X_{H2O} = a_{H2O}$ = 0.949
a_{H2O} = 1 U&T (1999)
Atg
Fo + Tlc
Atg
Fo + Tlc
ΔT,ΔP
500
600
700
T, °C